Estimation of flow and density using probe vehicles with spacing measurement equipment*

Toru Seo[†], Takahiko Kusakabe[‡], and Yasuo Asakura[§]

First submitted 14 July 2014; Accepted 30 January 2015

Abstract

Probe vehicles provide some of the most useful data for road traffic monitoring because they can acquire wide-ranging and spatiotemporally detailed information at a relatively low cost compared with traditional fixed-point observation. However, current GPS-equipped probe vehicles can not directly provide us volume-related variables such as flow and density. In this paper, we propose a new probe vehicle-based estimation method for obtaining volume-related variables by assuming that a probe vehicle can measure the spacing to its leading one. This assumption can be realized by utilizing key technologies in advanced driver assistance systems that are expected to spread in the near future. We developed a method of estimating the flow, density, and speed from the probe vehicle data without exogenous assumptions on traffic flow characteristics, such as a fundamental diagram. In order to quantify the characteristics of the method, we performed a field experiment at a real-world urban expressway by employing prototypes of the probe vehicles with spacing measurement equipment. The result showed that the proposed method could accurately estimate the 5 min and hourly traffic volumes with probe vehicle penetration rate of 3.5% and 0.2%, respectively.

keywords: probe vehicle; Lagrangian sensing; traffic flow; traffic state estimation; advanced driver assistance system

1 Introduction

Traffic observation is one of the most essential elements for the planning, management and control of transportation systems. It includes the observation of three fundamental variables—namely flow, density, and speed—also known as a traffic state (Daganzo, 1997). In general, the sufficient characteristics of a traffic state observation method can be described as follows:

- all of the fundamental variables (i.e., flow, density, and speed) can be simultaneously acquired,
- a spatially and/or temporally wide-ranging area can be covered,
- the spatial and/or temporal detailed information can be acquired, and
- accurate information can be acquired.

However, these characteristics are difficult to achieve simultaneously because of cost and technological limitations. Thus, different observation methods are applied to specific purposes based on their feasibility and information required. Reactive traffic controls such as ramp metering and signal control require spatiotemporally detailed information (e.g., on the speed, flow, and queue length) at target road sections (Papageorgiou et al., 2003). On the other hand, more macroscopic measures require information that is

*This is a manuscript of an article published in: Transportation Research Part C: Emerging Technologies, 53, 134–150, 2015, doi:10.1016/j.trc.2015.01.033

[†]Corresponding author. +81-3-5734-2575, Department of Civil Engineering, Tokyo Institute of Technology, 2-12-1-M1-20, O-okayama, Meguro, Tokyo 152-8552, Japan. t.seo@plan.cv.titech.ac.jp

[‡]t.kusakabe@plan.cv.titech.ac.jp

[§]asakura@plan.cv.titech.ac.jp

not so detailed but covers a wider range. For example, road network planning is based on the annual average daily traffic on major roads; and urban-scale macroscopic traffic management is expected to utilize the area flow and density (Geroliminis and Daganzo, 2008). For the efficient observation of traffic conditions, various methods have been proposed to date. Especially, recent achievements in information and communications technology (ICT) have enabled various information to be acquired by a wide variety of data collection methods. In the following paragraphs, we describe several conventional and emerging observation methodologies to demonstrate their capabilities.

Fixed-point observation methods can simultaneously acquire all the traffic state variables at their installed points. Roadside traffic detectors such as loop detectors are a typical equipment used for the method. Common detectors, such as loop detectors, can observe the flow and time occupancy at their installed points; then the density and speed can be estimated by putting weak assumptions such as average vehicle length and a steady speed in a short section. Video cameras can also be utilized as fixed-point observation and provide spatially detailed information near the installed points (e.g., Hilbert et al., 1980; Coifman et al., 1998). Therefore, the fixed-point observation methods can provide temporally detailed information at their installed points. However, information that is spatially detailed and wide-ranging is difficult to be acquired simultaneously; because the observable area of the methods is limited to the vicinity of the devices' installed points.

A probe vehicle is defined as having an onboard data collection devices that observes traffic conditions while the vehicle is in the traffic flow. Probe vehicle data can be analyzed to acquire wide-ranging and spatiotemporally detailed information; because they are often driven by travelers who range over the entire road network. Today, most common probe vehicles are the ones equipped with a Global Positioning System (GPS) device to identify their position and speed (e.g., Zito et al., 1995; Murakami and Wagner, 1999). From the GPS-equipped probe vehicle data, we can identify the probe vehicles' origins, destinations and routes by overlaid on a road map. Once these information are identified, the probe vehicle data directly provide the speed in road sections that the probe vehicles drove. Mobile communication devices and acceleration measurement devices have also been utilized as probes for specific purposes, such as indoor individual tracking and travel mode identification (e.g., Asakura and Hato, 2004; Reddy et al., 2010). Probe vehicle data have become popular with advances in ICT, and many studies have utilized them. For example, Herrera et al. (2010) evaluated detailed observation data from a large number of GPS-equipped probe vehicles on a highway. Yuan et al. (2012) developed an efficient traffic state estimation method based on Lagrangian observation and a Lagrangian-formulated traffic flow model, which they validated by using GPS-equipped probe vehicle data and a boundary fixed detector. However, GPS-equipped probe vehicle data do not provide the flow and density information; the significant limitation of them is that they cannot acquire volume-related information without strong exogenous assumptions, such as the fundamental diagram (FD) or the probe vehicle penetration rate. Wardrop and Charlesworth (1954) proposed a moving observer method that estimates the speed and flow of predetermined routes by using a single probe vehicle. The method relies on manually counting the number of vehicles that the probe vehicle overtakes, that overtake the probe vehicle, and that pass in the opposite direction, along with the journey time of the probe vehicle. Redmill et al. (2011) automated this method and showed that the method is capable of estimating the speed and vehicle class composition; however, the flow and density estimation has not been validated.

Recently, advanced driver assistance systems (ADAS), such as adaptive cruise control, collision avoidance, and autonomous vehicles, have been developed practically for the driving safety and efficiency purposes (c.f., National Highway Traffic Safety Administration, 2013). These systems automate some of the driving functions of vehicles. To realize ADAS, the surrounding environment of a vehicle must be recognized. This information, especially spacing (i.e., vehicle-to-vehicle distance), is valuable from the point of view of traffic observation; because spacing is equal to the inverse value of local density in the corresponding space. This information is impossible to be acquired with conventional probe vehicles, such as a GPS-equipped probe vehicle or Wardrop's moving observer. Therefore, ADAS-equipped vehicles are expected to be utilized as a source of data on volume-related information. The data can be automatically collected when the ADAS-equipped vehicle is being driven. Consequently, the data may enable wide-ranging and spatiotemporally detailed information to be obtained, including the flow and density, when enough ADAS-equipped probe vehicles are spread throughout a traffic system. A few studies

have examined this topic. Seo et al. (2012, 2013) developed such probe vehicle-based flow estimation methods; they validated the methods through simulation experiments. Yokoi et al. (2013) developed an onboard image recognition system that measures spacing that intended to utilized for traffic condition estimations.

The main objective of this study was to develop a new probe vehicle-based traffic estimation method that can derive volume-related variables where probe vehicles observe their surrounding vehicles with onboard equipments. In particular, we propose a method for estimating the flow, density, and speed variables based on the spacing data collected by the probe vehicles. The other objective was to verify the proposed method under actual traffic conditions by conducting a field experiment at a single predetermined corridor. By comparing the previous studies Seo et al. (2012, 2013), this study developed an estimation method that has higher applicabilities, investigated analytical characteristics of the method, and validated empirical characteristics of the method under actual traffic conditions. This paper consists of five sections. Section 2 presents the proposed estimation method of traffic flow variables (i.e., flow, density, and speed) using probe vehicle data. The estimation method is independent of exogenous assumptions such as FDs in order to exploit the advantages of observed spacing. Section 3 describes a field experiment that was conducted at an actual urban expressway and the probe vehicles with spacing measurement equipment. Section 4 presents the verification of the method, such as accuracy and precision of the estimation, resolution of acquired information, and probe vehicle penetration rate, based on the results of the field experiment.

2 Estimation method

We developed an estimation method based on data observed by probe vehicles with spacing measurement equipment. The method estimates the flow, density, and speed at a predetermined time and space resolution for a corridor that the probe vehicles drive through.

2.1 Assumptions and the concept of estimation method

The proposed estimation method is for traffic flow variables in a corridor. The corridor is assumed to be one-way traffic that can include multi-lane, merging, and diverging sections. Edie's generalized definitions (Edie, 1963) were employed for the traffic flow variables; these define the traffic flow variables (i.e., flow, density, and speed) in a time-space region based on the trajectories of all vehicles in the region and the area of the region. The definitions indicate generalized forms of the well-known traffic variable definitions, such as the spot flow rate, space density, and space mean speed.

The probe vehicle data are used as the inputs for the estimation. The data consist of the following continuously measured variables:

- spacing of the probe vehicle (i.e., space headway between the probe vehicle and its leading vehicle in the same lane) and
- position of the probe vehicle.

To simplify the situation, the following conditions are assumed:

- The measurements have no error.
- The route that the probe vehicle drives is identified without error.
- The probe vehicles are randomly distributed in the traffic; the penetration rate is unknown to analysts.
- The driving behavior of the probe vehicles is the same as that of other vehicles.

The first and second assumptions indicate an error free assumption. The third and fourth assumptions indicate a random sampling assumption.

The traffic flow estimation procedure is described as follows.

Step 1 Time-space region subject to the traffic state estimation is divided into multiple discrete time-space regions.

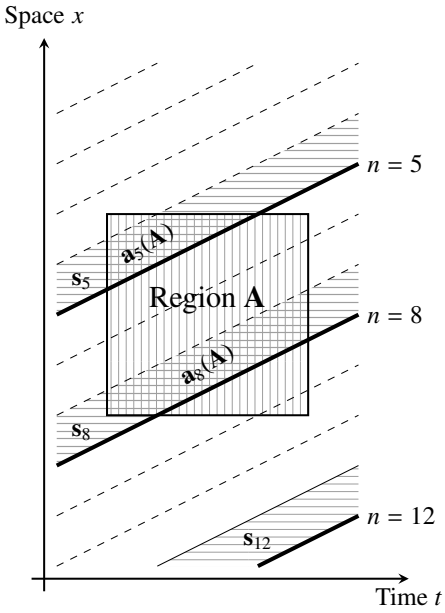

Figure 1: Time-space region **A** and probe vehicle data where the 5th, 8th and 12th vehicles are probes.

Step 2 The traffic flow variables of every time-space region are estimated independently based on data collected by the probe vehicles in each region.

Figure 1 shows a time-space diagram and time-space region, where the vertically hatched region **A** is a discrete time-space region, the thick solid lines are trajectories of the probe vehicles, the dashed lines are those of non-probe vehicles, and the horizontally hatched regions $\mathbf{s}_n$ are time-space regions between the n-th probe vehicle and its leading vehicle.

Any rule can be used to divide the time-space region of the traffic flow (step 1). The simplest rules is employed in this paper, where the traffic flow is divided into identical size of Eulerian rectangles. This is a familiar coordination in today's traffic flow data, where fixed-point detectors are installed at a certain time and space resolution or interval. This coordination can be represented as follows:

$$\mathbf{A}_i^j = \{(x,t) \mid x_i \le x \le x_{i+1},\ t_j \le t \le t_{j+1}\} \qquad i \ge 0,\ j \ge 0, \tag{1}$$

$$x_{i+1} = x_i + \Delta x, \tag{2}$$

$$t_{j+1} = t_j + \Delta t, \tag{3}$$

where i and j are non-negative indices for space and time, respectively, $(x_0,\ t_0)$ is the coordinates of a predetermined origin, $(x_i,\ t_j)$ is the coordinates of the lower-left corner of the region $\mathbf{A}_i^j$, Δx is a predetermined space resolution, and Δt is a predetermined time resolution. Note that $\mathbf{A}_i^j$ is simply written as **A** in the rest of this paper for the purpose of conciseness.

The estimation method of the step 2 is described in the next subsection.

2.2 Estimator formulation

The traffic flow variables defined by Edie (1963)—namely, the flow $q(\mathbf{A})$, density $k(\mathbf{A})$, and speed $v(\mathbf{A})$—in a time-space region **A** are as follows:

$$q(\mathbf{A}) = \frac{d(\mathbf{A})}{|\mathbf{A}|}, \tag{4}$$

$$k(\mathbf{A}) = \frac{t(\mathbf{A})}{|\mathbf{A}|}, \tag{5}$$

$$v(\mathbf{A}) = \frac{d(\mathbf{A})}{t(\mathbf{A})}, \tag{6}$$

where $d(\mathbf{A})$ is the total distance traveled by all of the vehicles in the region $\mathbf{A}$ [veh·km], $t(\mathbf{A})$ is the total time spent by all of the vehicles in the region $\mathbf{A}$ [veh·h], and $|\mathbf{A}|$ is the time-space area of the region $\mathbf{A}$ [km·h]. These definitions are easily transformed into (7)–(9) by summing the spacings and trajectories of each vehicle in the region $\mathbf{A}$:

$$q(\mathbf{A}) = \frac{\sum_{n\in\mathbf{N}(\mathbf{A})} d_n(\mathbf{A})}{\sum_{n\in\mathbf{N}(\mathbf{A})} |\mathbf{a}_n(\mathbf{A})|}, \tag{7}$$

$$k(\mathbf{A}) = \frac{\sum_{n\in\mathbf{N}(\mathbf{A})} t_n(\mathbf{A})}{\sum_{n\in\mathbf{N}(\mathbf{A})} |\mathbf{a}_n(\mathbf{A})|}, \tag{8}$$

$$v(\mathbf{A}) = \frac{\sum_{n\in\mathbf{N}(\mathbf{A})} d_n(\mathbf{A})}{\sum_{n\in\mathbf{N}(\mathbf{A})} t_n(\mathbf{A})}, \tag{9}$$

if $\sum_{n\in\mathbf{N}(\mathbf{A})} |\mathbf{a}_n(\mathbf{A})| > 0$, where $\mathbf{a}_n(\mathbf{A})$ is a time-space region between vehicle n and its leading vehicle in the region $\mathbf{A}$ ($\mathbf{a}_n(\mathbf{A}) = \mathbf{A} \cap \mathbf{s}_n$, cross-hatched regions in Figure 1), $\mathbf{N}(\mathbf{A})$ is a set of all vehicles in the region $\mathbf{A}$, $d_n(\mathbf{A})$ is the distance traveled by vehicle n in the region $\mathbf{A}$, and $t_n(\mathbf{A})$ is the time spent by vehicle n in the region $\mathbf{A}$.

By replacing $\mathbf{N}(\mathbf{A})$ in (7)–(9) with the set of all probe vehicles in region $\mathbf{A}$—namely, $\mathbf{P}(\mathbf{A})$—estimators based on the probe vehicle data can be defined as follows:

$$\hat{q}(\mathbf{A}) = \frac{\sum_{n\in\mathbf{P}(\mathbf{A})} d_n(\mathbf{A})}{\sum_{n\in\mathbf{P}(\mathbf{A})} |\mathbf{a}_n(\mathbf{A})|}, \tag{10}$$

$$\hat{k}(\mathbf{A}) = \frac{\sum_{n\in\mathbf{P}(\mathbf{A})} t_n(\mathbf{A})}{\sum_{n\in\mathbf{P}(\mathbf{A})} |\mathbf{a}_n(\mathbf{A})|}, \tag{11}$$

$$\hat{v}(\mathbf{A}) = \frac{\sum_{n\in\mathbf{P}(\mathbf{A})} d_n(\mathbf{A})}{\sum_{n\in\mathbf{P}(\mathbf{A})} t_n(\mathbf{A})}. \tag{12}$$

These estimators denote the flow, density, and speed of probe vehicles that works informal moving blockade. Note that (10)–(12) are exactly the same as (7)–(9) if all of the vehicles were the probe vehicles ($\mathbf{P}(\mathbf{A}) = \mathbf{N}(\mathbf{A})$).

The estimators represented in (10) and (11) are not unbiased in general. With third-order Taylor expansion, the bias in the flow and density estimators shown in (10) and (11) can be approximated as:

$$E[\hat{q}(\mathbf{A})] \simeq q(\mathbf{A}) + \frac{1}{|\mathbf{P}(\mathbf{A})|} \frac{Var[\bar{h}_n(\mathbf{A})]}{E[\bar{h}_n(\mathbf{A})]^3}, \tag{13}$$

$$E[\hat{k}(\mathbf{A})] \simeq k(\mathbf{A}) + \frac{1}{|\mathbf{P}(\mathbf{A})|} \frac{Var[\bar{s}_n(\mathbf{A})]}{E[\bar{s}_n(\mathbf{A})]^3}, \tag{14}$$

where $\bar{h}_n(\mathbf{A})$ and $\bar{s}_n(\mathbf{A})$ are the mean time and space headway, respectively, of vehicle n in the region $\mathbf{A}$ (see Appendix A for derivation of (13) and (14)). According to these equations, an inverse correlation exists between the bias and number of probe vehicles in the region. Therefore the bias tends to be mitigated as the size of the region is increased (i.e., time/space resolution is lowered) or the probe vehicle penetration rate is increased. The bias also correlates to the variance of all of the vehicles' mean time/space headway, which depends on the traffic flow characteristics. There is no bias in the speed estimator.

In a similar way, the precision of the flow and density estimators shown in (10) and (11) can be approximated as follows:

$$\mathrm{RMSE}(\hat{q}(\mathbf{A})) \simeq \frac{1}{E[\bar{h}_n(\mathbf{A})]^2} \sqrt{\frac{Var[\bar{h}_n(\mathbf{A})]}{|\mathbf{P}(\mathbf{A})|}}, \tag{15}$$

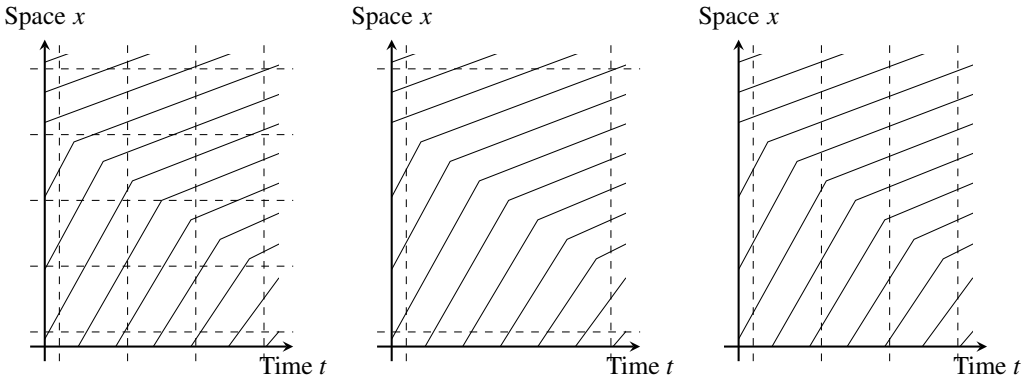

(a) Higher resolution (b) Lower resolution (c) MFD-like resolution

Figure 2: Examples of **A** shapes where the dashed lines represent each boundaries of **A**s.

$$\mathrm{RMSE}(\hat{k}(\mathbf{A})) \simeq \frac{1}{E[\bar{s}_n(\mathbf{A})]^2}\sqrt{\frac{Var[\bar{s}_n(\mathbf{A})]}{|\mathbf{P}(\mathbf{A})|}}, \tag{16}$$

where $\mathrm{RMSE}(\hat{\theta})$ is the root mean square error, which is a precision index of $\hat{\theta}$ (see Appendix B for derivation of (15) and (16)). The tendencies in the precision are quite similar to those in the bias; namely, the precision of the flow increases as the number of probe vehicles in a region increases and the variance in the mean time headway decreases.

2.3 Discussions on the method

With the method we can estimate the flow, density, and speed depending only on probe vehicle data. This characteristic is valuable for a traffic observation method because it makes wide-ranging data acquisition easy, as noted in Section 1. The method does not presume an FD, which is often used to estimate the traffic state in existing studies (e.g., Nanthawichit et al., 2003; Yuan et al., 2012; Mehran et al., 2012). Because of this independency from an FD, the results obtained with this method are robust against unpredictable or uncertain factors of traffic flow, such as traffic incidents. In addition, the results can be utilized to estimate or calibrate traffic flow models, including FDs.

The resolution of the estimation (Δt and Δx) can be adjusted to the requirements by the planners and analysts. As shown in (13)–(16), there is a tradeoff between the estimation accuracy and precision and resolution, as well as a positive relation between the accuracy and precision and probe vehicle penetration rate. Therefore, analysts can choose a desired resolution depending on the estimation purpose and the number of probe vehicles in order to maintain the required accuracy and precision. Figure 2 illustrates examples of the shapes of **A**. If the number of probe vehicles is sufficiently large, a high resolution can be set—detailed and dynamic changes in traffic states can be recognized (Figure 2(a)). In contrast, even if the number of probe vehicles is very small, analysts can still obtain some knowledge on the traffic by setting a low resolution, such as an hourly traffic volume (Figure 2(b)) and area density (Macroscopic Fundamental Diagrams (MFD), Figure 2(c)). We quantitatively analyzed these relation among accuracy and precision of the estimation, time and space resolution, and probe vehicle penetration rate which we discuss in Section 4, based on a field experiment that we describe in Section 3.

The proposed method relies on assumptions that may not always satisfied in the real world, namely the error free and random sampling assumptions (c.f., Section 2.1). The error free assumption can be reasonable except in situations with very sparse traffic where a leading vehicle is not detectable. The reasons are as follows. Small errors in position measurement[1] do not significantly affect accuracy and precision

[1] Usual GPS-based map-matching techniques' accuracy is around 10 m (Quddus et al., 2007).

of the proposed method. If the size of the time-space region $\mathbf{A}$ is larger enough than expected error in position measurement, errors in $d_n(\mathbf{A})$, $t_n(\mathbf{A})$ and $\mathbf{a}_n(\mathbf{A})$ can be neglectable. On the other hand, errors in spacing measurement directly affect $\mathbf{a}_n(\mathbf{A})$ and accuracy and precision of the proposed method. However, errors in spacing measurement should be small because practically implemented spacing measurement technologies have to provide good features in order to guarantee the safety of the ADAS[2]. Although the spacing measurement requires assumption on vehicle length, this can be only a weak assumption; because variation of vehicle length is expected to be relatively smaller comparing to that of the spacing.

The random sampling assumption may not always satisfied in the real world. This means that the probe vehicles may have different driving behaviors compared with other vehicles. In general, the estimation biases caused by biases in probe vehicles' driving behavior can be explained as follows. Let r_1 and r_2 be positive coefficients describing the biases on speed and spacing respectively. If the probe vehicle's speed is r_1 times the average speed of all the vehicles, the flow and speed will be estimated r_1 times the actual state. If the probe vehicle's spacing is r_2 times the average spacing of all the vehicles, the flow and density will be estimated $1/r_2$ times the actual state.

3 Field experiment

In this section, we describe a field experiment conducted under actual traffic conditions.

The field experiment was conducted on Tuesday, September 24, 2013, from 15:00 to 16:00. The location was the counterclockwise direction in the Inner Circular Route of the Metropolitan Expressway, which is an urban expressway in Tokyo, Japan. The weather was cloudy with occasional light rain. Twenty probe vehicles equipped with spacing and position measurement devices were employed.

3.1 Inner Circular Route

The Inner Circular Route (i.e., C1) is a ring-shaped urban expressway located in central Tokyo. In the experiment, the probe vehicles ran in the counterclockwise direction. The loop length is 14.2 km, and most sections have two lanes for cruising and passing. The speed limit is 50 km/h. Figures 3 and 4 show a map and a schematic of C1, respectively. The space coordinates denoted in Figure 4 are used throughout this paper. In Figure 4, a junction is abbreviated as JCT, arrows on the upper side represent the merging from or diverging to other highway routes, and arrows on the lower side represent on/off ramps. Note that the survey section was limited to an 11 km length section from the 0 km point to the 11 km point, because a series of tunnels at the 11–14.2 km disturbed the GPS functions.

A large number of dual supersonic traffic detectors are installed in C1. They enable us to obtain highly detailed and accurate data on the traffic flow variables[3]. The traffic detectors observed the flow, spot speed, and spot occupancy directly, and these were converted to density and speed for validation of the proposed method. The observation with the traffic detectors is performed at a time resolution of 1 min and average space resolution of 250 meters per lane. In this study, these detector observed data are used for comparison purposes. Figure 5 shows the density observed by the detectors in the cruising lane as a time-space diagram; where the horizontal axis indicates the time and future is to the right, the vertical axis indicate space and downstream is in the upward direction. Some remarkable events were occurred during the experiment. For example, Edobashi JCT at the 8 km point become a merging bottleneck and caused a 3 km queue was formed at 15:50. Queue spillovers from other highway routes were observed via Takebashi JCT at the 10 km point and Hamazakibashi JCT at the 3.8 km point.

[2]For example, Saneyoshi (1996), which utilized stereo camera and was commercialized recently, reported that the precision is within ±0.01 m and ±1 m at distances of 5 m and 100 m, respectively. The maximum detectable range is 130 m.

[3]Shiraishi et al. (2012) reported that measurement error in 5 min flow of a dual supersonic traffic detector was usually less than 10%.

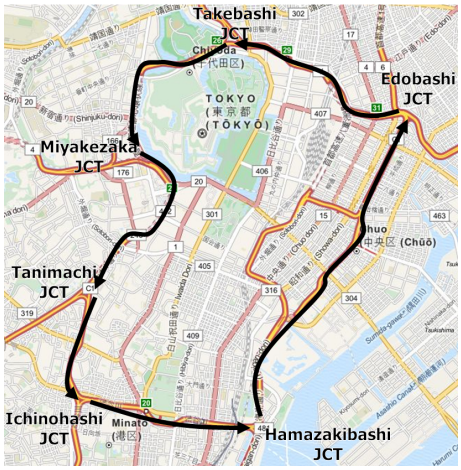

Figure 3: Map of the Inner Circular Route.

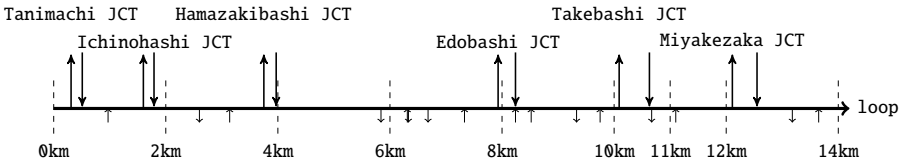

Figure 4: Schematic of the Inner Circular Route (counterclockwise direction).

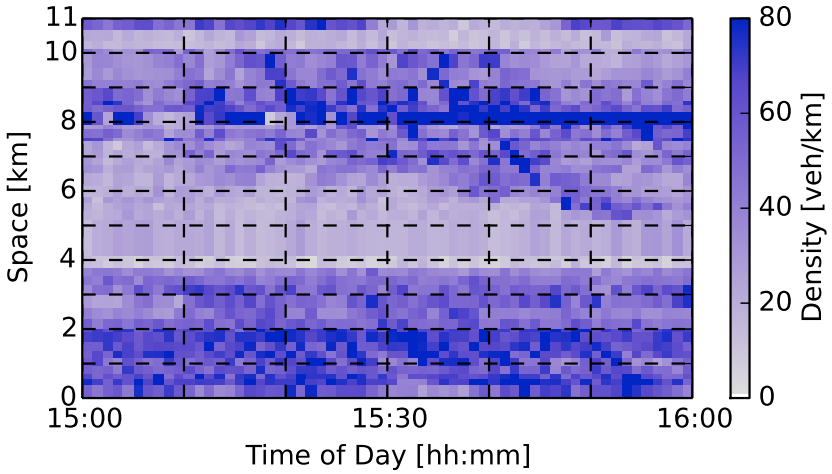

Figure 5: Time-space diagram of density in C1 as observed by the detectors.

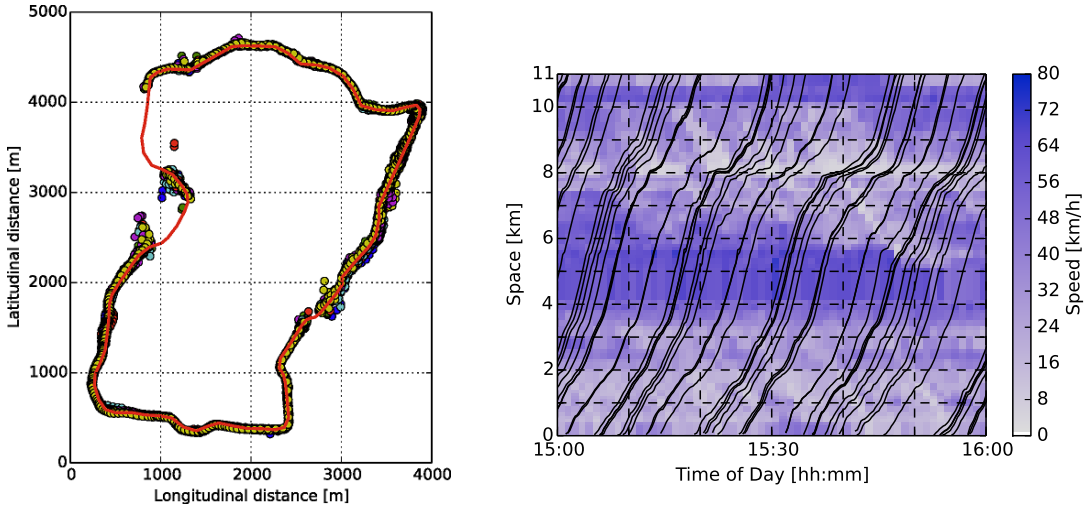

(a) Raw data of trajectories plotted on a map

(b) Map-matched trajectories on time-space diagram of speed

Figure 6: Trajectories of probe vehicles.

3.2 Probe vehicle data

Twenty standard-sized passenger vehicles with non-professional drivers were employed as the probe vehicles. The vehicles were equipped with mono-eye cameras and GPS loggers on their dashboards to identify and record the spacing and position. The survey section was limited to the cruising lane of the 0–11 km section because of law restrictions[4] and the GPS function. Most of the probe vehicles drove three laps on C1, and a total of 59 laps were performed during the experiment period. This corresponded to 42.1 veh/h/lane. The flow of all vehicles in the survey section of C1 was 1,255.2 veh/h/lane according to the detector data. Therefore, the probe vehicle penetration rate was roughly calculated to 3.5%[5]. Probe vehicle data, including positions and spacing, were collected at intervals of 15 s. Thus, an average number of 38.8 data points was recorded per lap.

Vehicle positions were identified by the GPS data and simple map-matching procedure. The procedure is described as follows: 1) a digital map consists of the experiment site of links and nodes was acquired from an external source; 2) vehicle coordinates identified by GPS were matched to their closest point on the links; 3) data points located at 11–14.2 km section where the series of tunnels exist were removed. Figure 6 shows the trajectories of the probe vehicles. Figure 6(a) shows the raw data plotted on a map of C1 where the red solid line indicates the shape of C1 and small circles indicate the vehicle coordinates. According to the figure, the measurement errors were not significant excluding tunnels. Figure 6(b) shows the map-matched data on the time-space diagram with speed; the trajectories seemed to be reasonable. For example, the probe vehicles tended to be slow (i.e., the slopes of trajectories decreased) when they went through the bottleneck at the 8 km point just like other vehicles (i.e., the plot color was dark). Although small errors were found in the GPS measurement and map-matching, the proposed traffic state estimation method is not significantly affected by such small errors as mentioned in Section 2.3.

This study employs a spacing measurement method using a mono-eye camera equipped on the dashboard of the probe vehicles. Figure 7 shows some images taken by the cameras on the probe vehicles during the experiment; typical road environments and vehicle characteristics at the C1 are shown. The procedure of the spacing measurement method is described as follows: 1) the leading vehicles of the probe vehicles in the image were identified; 2) the apparent size of the leading vehicles' body width were

[4] According to Japan's Road Traffic Act, vehicles should drive in the cruising lane unless changing routes, overtaking within the speed limit, or avoiding danger.

[5] The 5% penetration rate was set as the target experiment size by referring to simulation results of previous studies Seo et al. (2012, 2013). They suggested that 5% may be sufficient under similar conditions.

Figure 7: Examples of images taken by the cameras on the probe vehicles.

Table 1: Spot speed and spacing statistics of probe vehicle data and detector data.

		0.390 km point	2.980 km point	7.140 km point	8.640 km point
Speed	Detector data (μ, σ) [km/h]	(24.2, 10.7)	(25.8, 10.5)	(26.3, 11.4)	(29.7, 9.3)
	Probe vehicle data (μ, σ) [km/h]	(27.7, 11.8)	(28.4, 6.8)	(29.5, 10.2)	(26.2, 11.0)
	K–S test value $\sqrt{n}D_n$	0.684	1.248	0.763	1.568
Spacing	Detector data (μ, σ) [m]	(19.4, 11.2)	(19.2, 11.7)	(20.7, 12.3)	(21.5, 11.8)
	Probe vehicle data (μ, σ) [m]	(21.8, 11.5)	(22.4, 9.9)	(24.5, 11.4)	(19.7, 8.5)
	K–S test value $\sqrt{n}D_n$	1.008	1.784	1.503	0.518

measured; 3) the spacing were calculated based on the apparent size, its assumed actual size, angle of view of camera, etc. (see Appendix C for the detail). If assumed or measured variables have errors, the estimated spacing will have errors. We can not determine the amount of the errors; because the ground truth data for the vehicle size during the experiment do not exist. However, the method may not be biased significantly and practicable for the experimental measurement because the assumed variables were based on common knowledge on statistics and regulations and detector data. In addition to that, the measurement was based on high resolution images. The reason for the simple method is because implementation is relatively easy and they satisfy the requirement for this experiment. That is, the method is

- capable of detecting the leading vehicle at relatively long distance that often appears in highways,
- capable of determining the lane driven by the probe vehicle and the leading vehicle, and
- based on a clear logic (i.e., not a black box).

Note that any methods of measuring spacing are considerable for the proposed traffic state estimation methodology as long as the measurement method satisfies the required capability.

In order to validate the probe vehicle data, we compared the data with the spacing and spot speed of all of the vehicles at four specific locations as calculated by the detectors' pulse data[6]. Figures 8 and 9 show the speed and spacing distributions. Their statistics (mean μ, standard deviation σ, and Kolmogorov–Smirnov (K–S) test value $\sqrt{n}D_n$) are summarized in Table 1. If the K–S test value is larger than 1.36, the difference between probe vehicle data and detector data is statistically significant at the 5% level. According to these comparisons, there considered to be differences between the two data at some locations. The probe vehicles had slightly faster speed and larger spacing at the three points (0.390 km, 2.980 km and 7.140 km points), and the reverse occurred at the 8.640 km point. The probe vehicles' routes were assigned to maintain cruising lane, therefore, their driving behavior may have slightly differed from that of other vehicles of which paths were going to diverge or had just merged. For example, the 8.640 km point was located downstream of the merging at Edobashi JCT (c.f., Figure 4). At this location, vehicles from C1 are often required to slow down to merge because of its road alignment. Therefore, the probe vehicles may have tended to be slower than other vehicles. Because of these reasons, the probe vehicle data may contain location-specific biases. This means that the random sampling assumption was not rigorously satisfied in the experiment.

[6]The detectors' pulse data include every individual vehicle's spot speed, body length, and time headway at the detector location.

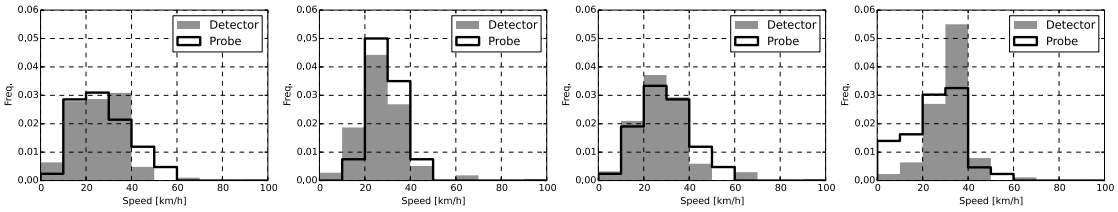

(a) At 0.390 km point. (b) At 2.980 km point. (c) At 7.140 km point. (d) At 8.640 km point.

Figure 8: Spot speed distributions in probe vehicle data and detector data.

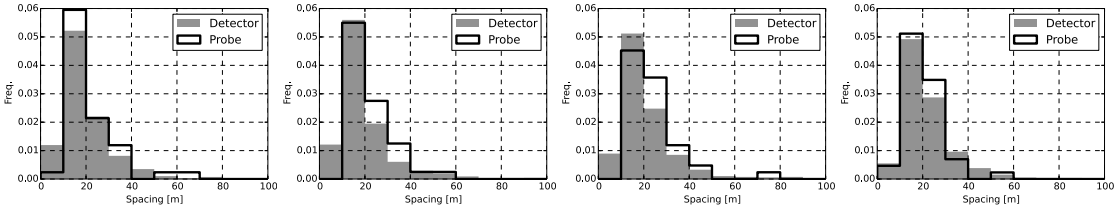

(a) At 0.390 km point. (b) At 2.980 km point. (c) At 7.140 km point. (d) At 8.640 km point.

Figure 9: Spacing distributions in probe vehicle data and detector data.

4 Empirical analysis

We quantitatively analyzed the estimation results based on the proposed method presented in Section 2 and collected data presented in Section 3. Section 4.1 visualize examples of estimation results as time-space diagrams in order to investigate how well the traffic phenomena can be reproduced by the proposed method. Section 4.2 summarizes indices for accuracy and precision of the proposed method for various settings of the probe vehicle penetration rate and the resolution. Section 4.3 describes relation between accuracy and precision of the proposed method and the traffic state.

4.1 Visualizations of estimation results

Figure 10 visualizes traffic states estimated by the proposed method (left side: a, c, e), as well as ones observed by the detectors (right side: b, d, f). The time and space resolution of the estimation were set to 5 min and 500 m, respectively, that is close to average distance between detectors and detector's data aggregation time interval in urban expressways in Japan. The probe vehicle penetration rate was 3.5%. At this resolution and penetration rate, the expected number of probe vehicles per region was 3.83; therefore, bias in the estimator is expected to be small (c.f., Section 2.2). Traffic phenomena that were observed in the traffic detector data could be recognized in this estimation result. For example, Figure 10(c) shows a significant queue whose head was at the 8 km point and that propagated to a length of around 3 km at 15:50. There were other congested areas whose heads were at around the 3.5 km and 10 km points. These characteristics were almost identical to those described in Section 3.1 and Figure 10(d) by the detector data.

The resolution of the estimation can be set flexibly corresponding to the objective of the analysis and probe vehicle penetration rate (c.f., Section 2.3). Lower probe vehicle penetration rate scenarios were generated from random sampling of the probe vehicles. Figure 11(a) shows the density estimation result at a resolution of 30 min and 4 km with a 1% probe vehicle penetration rate; Figure 11(b) shows the density observed by the detectors aggregated with the corresponding resolution. The estimation results showed the tendencies of the traffic flow at lower resolutions. For example, the 0–4 km section had a relatively dense traffic flow, while the 4–8 km section tended to have sparse traffic at 15:00–15:30 and dense traffic at 15:30–16:00.

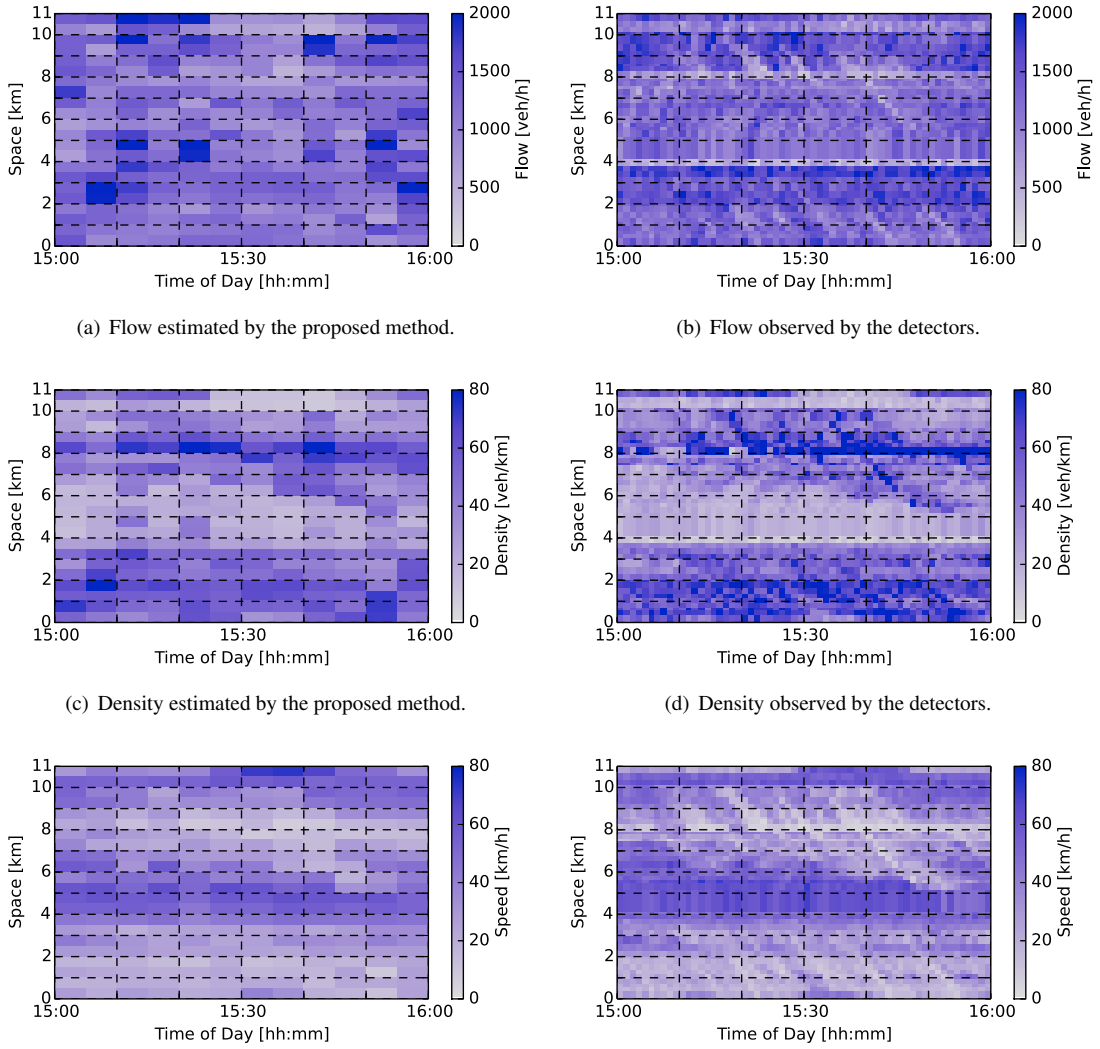

(a) Flow estimated by the proposed method.

(b) Flow observed by the detectors.

(c) Density estimated by the proposed method.

(d) Density observed by the detectors.

(e) Speed estimated by the proposed method.

(f) Speed observed by the detectors.

Figure 10: Visualization of estimated flow, density, and speed.

4.2 Relation among accuracy and precision of the estimation, resolution, and probe vehicle penetration rate

To quantify the relations among accuracy and precision of the estimation, time and space resolution, and probe vehicle penetration rate, we compared accuracy and precision indices for the estimation scenarios. The bias and the root mean square percentage error (RMSPE) are employed as accuracy and precision indices, where $\mathrm{Bias}(\hat{\theta}) = E[\hat{\theta} - \theta]$ and $\mathrm{RMSPE}(\hat{\theta}) = \sqrt{E[((\hat{\theta} - \theta)/\theta)^2]}$. Variable θ denotes a traffic flow variable (one of q, k and v) at a certain time and space observed by the detectors; and variable $\hat{\theta}$ is one of those estimated from the probe vehicle data. In addition to that, analytically expected bias and precision shown in (13)–(16), namely $\widehat{\mathrm{Bias}}(\hat{\theta})$ and $\widehat{\mathrm{RMSPE}}(\hat{\theta})$, were estimated for every scenario. The estimation was based on (13)–(16) by estimating expectation of mean and variance spacing and time headway from the probe vehicle data. The parameters set for scenarios were probe vehicle penetration rate P [%], time resolution Δt [min], and space resolution Δx [km]. The probe vehicle penetration rate P was 3.5% or 0.2%.

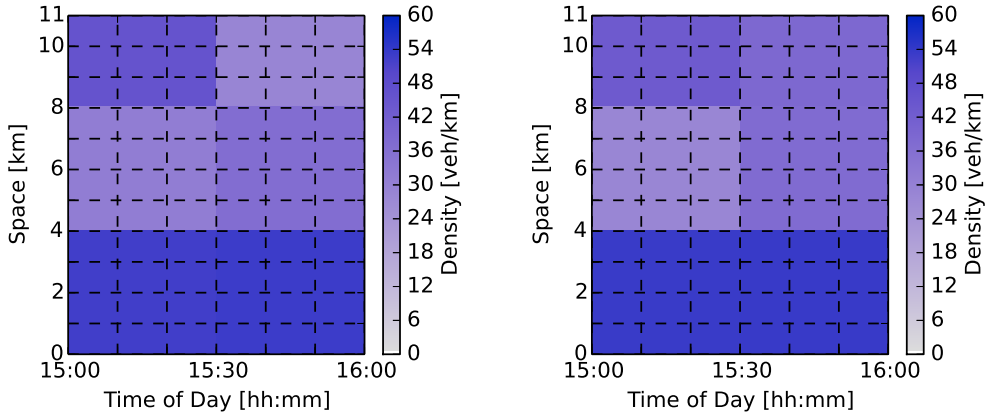

(a) Density estimated by the proposed method

(b) Density observed by the detectors

Figure 11: Visualization of estimated density with lower resolution (30 min×4 km) and lower probe vehicle penetration rate (1%)

In scenarios where $P = 3.5\%$, data from all of the probe vehicles were used for the estimation. In scenarios where $P = 0.2\%$, data from two randomly sampled laps were used on average (i.e., the expected flow of probe vehicles is 2 veh/h). The indices for the lower penetration rate scenarios were calculated from the results of 20 estimation iterations. In each iteration, probe vehicle data for the estimation were composed of different combinations of probe vehicles' laps whose penetration rate was expected to be the scenario parameter P. The time resolution Δt was 5 min or 60 min, which corresponded to the resolutions used for Japanese highway traffic management and traffic census data, respectively. The space resolution Δx was 0.5 km or 11 km, which roughly corresponded to the usual detector interval and entire survey section length, respectively. For results of more various scenarios, such as 1 min time resolution, see Appendix D.

Table 2 summarizes the results of above estimation. Note that the mean values of the flow, density, and speed observed by the detectors were 1,255.2 veh/h, 40.7 veh/km and 30.8 km/h, respectively.

The biases were affected by three different factors: the analytical characteristics of the estimators (c.f., (13) and (14), Section 2.2), biases in the probe vehicles' driving behavior (c.f., Section 2.3 and 3.2), and biases in the spacing measurement method (c.f., Section 3.2 and Appendix C). According to Table 2, amounts of the analytical expected biases, $\widehat{\mathrm{Bias}}(\hat{\theta})$, were almost negligible compared with the amounts of states for most of scenarios. However, the actual biases on the flow and density calculated from the detector data were not identical to the analytically expected ones. For example, most of the actual biases were negative while the analytical expected one is positive. This can be explained by the probe vehicles' driving behavior biases as follows. In the (3.5%, 60 min, 11 km) scenario, whose analytically expected bias is small, slightly underestimated the flow, density, and speed. This suggests that the probe vehicles' driving behavior was slightly biased compared with the rest of traffic (c.f., Section 2.3): the probe vehicles had 10% slower speed than other vehicles on average, and they had almost the same spacing with other vehicles on average. The amount of bias caused by the spacing measurement method can be expected to be small as mentioned in Section 3.2.

The tendencies in the precision RMSPE can be found as analytically expected; the precision improves as P, Δt and Δx increased. However, the actual precision was lower than the analytically expected one in most of the scenarios. This is also able to be explained by the probe vehicles' driving behavior biases. Therefore, if biases in the probe vehicle data did not exist (i.e., if the random sampling assumption were satisfied), RMSPE is expected to improve.

4.3 Relations among accuracy and precision of the estimation, and traffic state

Figure 12 compares the estimated variables and the corresponding values observed by the detectors based on the results of the (3.5%, 5 min, 0.5 km) scenario. The colors represent the number of cases. The

Table 2: Precision and bias indices over estimation scenarios.

(a) Flow.

Scenario parameters			Errors against the detector data		Analytically expected errors	
P (%)	Δt (min)	Δx (km)	RMSPE($\hat{q}$) (%)	Bias($\hat{q}$) (veh/h)	$\widehat{\text{RMSPE}}(\hat{q})$ (%)	$\widehat{\text{Bias}}(\hat{q})$ (veh/h)
0.2	5	0.5	43	21.1	67	111.5
0.2	5	11	33	-48.7	25	26.6
0.2	60	0.5	25	-59.9	27	37.3
0.2	60	11	16	-159.0	13	29.6
3.5	5	0.5	26	-82.4	17	42.6
3.5	5	11	14	-151.9	7	5.2
3.5	60	0.5	14	-147.1	6	4.5
3.5	60	11	13	-161.4	3	1.2

(b) Density.

Scenario parameters			Errors against the detector data		Analytically expected errors	
P (%)	Δt (min)	Δx (km)	RMSPE($\hat{k}$) (%)	Bias($\hat{k}$) (veh/km)	$\widehat{\text{RMSPE}}(\hat{k})$ (%)	$\widehat{\text{Bias}}(\hat{k})$ (veh/km)
0.2	5	0.5	49	-0.1	69	4.1
0.2	5	11	45	2.1	27	3.3
0.2	60	0.5	28	-2.9	44	1.3
0.2	60	11	13	-1.1	17	1.1
3.5	5	0.5	28	-2.6	17	1.2
3.5	5	11	15	-0.6	11	0.5
3.5	60	0.5	14	-4.2	7	0.2
3.5	60	11	3	-1.4	4	0.1

(c) Speed.

Scenario parameters			Errors against the detector data	
P (%)	Δt (min)	Δx (km)	RMSPE($\hat{v}$) (%)	Bias($\hat{v}$) (km/h)
0.2	5	0.5	43	0.4
0.2	5	11	31	-0.3
0.2	60	0.5	23	0.7
0.2	60	11	11	-3.1
3.5	5	0.5	18	-0.7
3.5	5	11	13	-3.0
3.5	60	0.5	12	-0.6
3.5	60	11	10	-3.0

estimated variables correlated well with the corresponding values observed by the detectors in most cases. However, the relative error for the density tended to be larger when the density was low. This may be due to the variances in the mean headway. The variances tended to be larger at lower densities than at higher densities, and the accuracy and precision may have suffered, as suggested by (13)–(16) in Section 2.2. This means that the estimation accuracy and precision depend on the traffic state, although the amount of error was not significant among traffic states from free flow to congested flow.

Note that the data do not contain situations where the flow was low, such as sparse traffic, extremely congested traffic, and signalized traffic. Therefore, the capabilities of the method in such situations were not validated with this data. According to Section 2.2, the accuracy and precision may decrease for sparse traffic and signalized traffic because of the larger variance in the mean headway distribution.

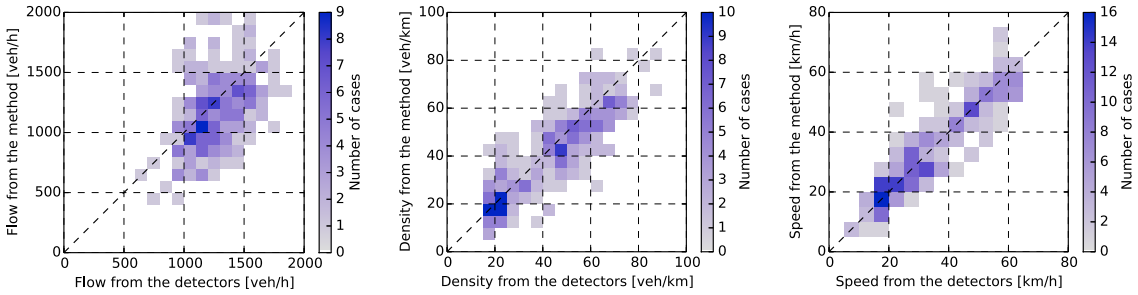

(a) Flow. (b) Density. (c) Speed.

Figure 12: Scatter plots of estimated variables versus the corresponding values observed by the detectors.

5 Conclusion

In this paper, we proposed a new method to acquire volume-related variables from probe vehicle data and presented an empirical examination of its feasibility. The method relies on the utilization of on-vehicle spacing measurement technologies that are likely to spread in the near future because they are key components of ADAS.

We developed an estimation method of traffic flow variables based on the proposed probe vehicle data. The method estimates the flow, density, and speed in predetermined time-space regions based on observed spacings and positions of some of the vehicles in each region. The shape of the predetermined time-space region is at the discretion of the planners and analysts; therefore, various time and space resolutions of the information can be acquired. The accuracy and precision of the flow and density estimation correlate to the number of probe vehicles in the time-space region; therefore, the resolution level should be adjusted according to the desired information accuracy and precision and number of probe vehicles. The developed method does not rely on any exogenous assumptions on the traffic flow characteristics, such as an FD. This makes the method highly robust against unpredictable or uncertain traffic phenomena, such as traffic incidents (i.e, traffic accidents affect flow capacity, free flow speed, etc.) and the effect of advanced technologies in the future (e.g., platooning, zero reaction time due to automation). In addition, the method can be utilized to estimate traffic flow models including FDs.

The method was quantitatively validated based on the results of a proof-of-concept field experiment. The field experiment was conducted at an urban expressway in Tokyo using twenty probe vehicles with spacing measurement equipments. The relation among the accuracy and precision of the estimation, probe vehicle penetration rates, time and space resolutions, and traffic states were examined by comparing the estimation result based on the probe vehicle data, and the detector data. One of the advantages of field experiment-based validation compared with microscopic simulator-based validation that were utilized by the previous studies Seo et al. (2012, 2013) is that we do not need to discuss about traffic flow models such as car following models—which have significant relation to the proposed method.

Our findings are summarized as follows. The proposed probe vehicle-based estimation method is capable of estimating the flow and density well. The accuracy and precision of the estimation are strongly related to the time and space resolutions of the estimation and the probe vehicle penetration rate . For example, according to the results of the field experiment for a partially congested urban expressway, if the probe vehicle penetration rate is 3.5%, the proposed method estimated detailed information that represents dynamic phenomena, such as queue existence and propagation. However, even with the penetration rate of 3.5%, the proposed method's precision was not very practically good for higher resolution information such as 5 min flow that are often employed at traffic management and control. On the other hand, with a lower probe vehicle penetration rate of 0.2% (i.e., two probe vehicles per hour), the proposed method was able to estimate lower resolution information, such as hourly traffic volume. Note that the probe vehicle data we used in this study contain small biases, such as the driving behavior and measurement of the spacings; the results suggest that the estimation accuracy may be improved if the biases in the data do not exist. These

results implies that the proposed method has good potential to be utilized for a transportation planning purposes with probe vehicle penetration rate of several percents. For traffic management and control purposes, the proposed method may require higher penetration rate; considering possibility of spread of ADAS in the future, such high penetration rate might be realized. The authors do not insist that the proposed method could replace all the existing methods (e.g., fixed-point observation). However, the method can be used in areas where any sensors have not been installed yet. It will enable us to expand observation fields. In addition to that, we confirmed that the proposed method had better precision than a GPS-equipped probe vehicle-based estimation method with a certain exogenous knowledge, namely average probe vehicle penetration rate (see Appendix E).

Several future works are planned. The first is to improve the estimators. The estimators formulated in (10) and (11) are biased. The second-order term in the Taylor series of (13) and (14) may be valuable in formulating less biased estimators. The second is to develop a method for better resolving the time-space regions (step 1 in Section 2.1) rather than the simple method in this paper. The third is to develop a model that describes the interdependencies between consecutive time-space regions, by employing a traffic flow model whose parameters (e.g., an FD) are endogenously estimated from the probe vehicle data. The fourth is to develop an unbiased estimation method that can be applied to biased probe vehicle data. This is an important topic because the ADAS may cause biases in the probe vehicles' driving behavior. Use of information on the surrounding vehicles of the probe one, which are expected to be not biased, may be valuable to obtain the unbiased estimation. For example, replacing $d_n(\mathbf{A})$ and $t_n(\mathbf{A})$ in the estimators with the leading vehicle's distance traveled/time spent in $\mathbf{A}$ might decrease bias in the estimators. The fifth is to validate the proposed method with microscopic traffic flow simulation. Although a simulator has some limitations as mentioned before, its advantages should not be abandoned; it can reproduce various traffic situation and can control measurement errors and biases in driving behavior. Therefore, carefully prepared simulations might complement the validation.

Acknowledgments

The traffic detector data was kindly provided by Metropolitan Expressway Co., Ltd. We would like to thank Prof. Carlos F. Daganzo (University of California, Berkeley) for his valuable advice on the estimation method, Ms. Kiko Yamada-Kawai (Tokyo Institute of Technology) and anonymous reviewers for their insightful comments on the earlier versions of this paper, Mr. Shuichi Yamaguchi (Japan Expressway International Co., Ltd.), Dr. Hiroshi Warita (Metropolitan Expressway Co., Ltd.), Dr. Yasuhiro Nonaka and Mr. Takashi Ishida (Highway Planning Co., Ltd.) for their technical advice on the field experiment, and Survey Research Center Co., Ltd. for their technical and professional assistance with the experiment. Part of this work was financially supported by the Research Fellow (DC2) program of the Japan Society for the Promotion of Science (KAKENHI Grant-in-Aid for JSPS Fellows #26010218).

Appendix A: Analytical derivation of bias in estimation

This appendix presents an analytical derivation of the amount of bias in the flow estimator given in (13).

The approximation of $|\mathbf{a}_n(\mathbf{A})| \simeq d_n(\mathbf{A})\bar{h}_n(\mathbf{A})$ can be appropriate for most situations, such as when the size of region $\mathbf{A}$ is sufficiently larger than the spacing. With this approximation, the true flow in (7) can be transformed to

$$q(\mathbf{A}) \simeq \frac{E[d_n(\mathbf{A})]}{E[d_n(\mathbf{A})\bar{h}_n(\mathbf{A})]}. \tag{A.1}$$

We assumed that $d_n(\mathbf{A})$ and $\bar{h}_n(\mathbf{A})$ are independent from each other. Therefore,

$$q(\mathbf{A}) \simeq \frac{1}{E[\bar{h}_n(\mathbf{A})]}. \tag{A.2}$$

In the same way, the flow estimator in (10) can be transformed to

$$\hat{q}(\mathbf{A}) \simeq \frac{1}{E_{\mathbf{P}(\mathbf{A})}[\bar{h}_n(\mathbf{A})]}, \tag{A.3}$$

where $E_{\mathbf{P}(\mathbf{A})}[\theta_n]$ is the mean of θ_n for each vehicle in $\mathbf{P}(\mathbf{A})$. The expected value of the estimator is

$$E[\hat{q}(\mathbf{A})] \simeq E\left[\frac{1}{E_{\mathbf{P}(\mathbf{A})}[\bar{h}_n(\mathbf{A})]}\right]. \tag{A.4}$$

The third-order Taylor expansion of $f(X) = 1/X$ around $E[X]$ is derived as

$$\frac{1}{X} \simeq \frac{1}{E[X]} - \frac{1}{E[X]^2}(X - E[X]) + \frac{1}{E[X]^3}(X - E[X])^2 - \frac{1}{E[X]^4}(X - E[X])^3. \tag{A.5}$$

We can then obtain

$$E\left[\frac{1}{E_{\mathbf{P}(\mathbf{A})}[\bar{h}_n(\mathbf{A})]}\right] \simeq \frac{1}{E[E_{\mathbf{P}(\mathbf{A})}[\bar{h}_n(\mathbf{A})]]} + \frac{Var[E_{\mathbf{P}(\mathbf{A})}[\bar{h}_n(\mathbf{A})]]}{E[E_{\mathbf{P}(\mathbf{A})}[\bar{h}_n(\mathbf{A})]]^3}, \tag{A.6}$$

by taking the expectations and substituting $E_{\mathbf{P}(\mathbf{A})}[\bar{h}_n(\mathbf{A})]$ for X. If the probe vehicles are randomly sampled from all of the vehicles, $E[E_{\mathbf{P}(\mathbf{A})}[\bar{h}_n(\mathbf{A})]] = E[\bar{h}_n(\mathbf{A})]$ and $Var[E_{\mathbf{P}(\mathbf{A})}[\bar{h}_n(\mathbf{A})]] \simeq Var[\bar{h}_n(\mathbf{A})]/|\mathbf{P}(\mathbf{A})|$ are satisfied. Therefore, (A.6) can be transformed to

$$E\left[\frac{1}{E_{\mathbf{P}(\mathbf{A})}[\bar{h}_n(\mathbf{A})]}\right] \simeq \frac{1}{E[\bar{h}_n(\mathbf{A})]} + \frac{1}{|\mathbf{P}(\mathbf{A})|}\frac{Var[\bar{h}_n(\mathbf{A})]}{E[\bar{h}_n(\mathbf{A})]^3}. \tag{A.7}$$

From (A.2), (A.4), and (A.7), the relation between flow and its estimator can be approximated as

$$E[\hat{q}(\mathbf{A})] \simeq q(\mathbf{A}) + \frac{1}{|\mathbf{P}(\mathbf{A})|}\frac{Var[\bar{h}_n(\mathbf{A})]}{E[\bar{h}_n(\mathbf{A})]^3}. \tag{A.8}$$

Appendix B: Analytical derivation of precision of estimation

This appendix presents an analytical derivation of the precision of the flow estimator given in (15).

The index for the precision—namely, root mean square error (RMSE)—is represented as follows:

$$\begin{aligned}
\mathrm{RMSE}(\hat{q}(\mathbf{A})) &= \sqrt{E[(q(\mathbf{A}) - \hat{q}(\mathbf{A}))^2]} \\
&\simeq \sqrt{E\left[\left(\frac{1}{E[\bar{h}_n(\mathbf{A})]} - \frac{1}{E_{\mathbf{P}(\mathbf{A})}[\bar{h}_n(\mathbf{A})]}\right)^2\right]} \\
&= \sqrt{E\left[\frac{1}{E[\bar{h}_n(\mathbf{A})]^2}\right] - E\left[\frac{2}{E[\bar{h}_n(\mathbf{A})]E_{\mathbf{P}(\mathbf{A})}[\bar{h}_n(\mathbf{A})]}\right] + E\left[\frac{1}{E_{\mathbf{P}(\mathbf{A})}[\bar{h}_n(\mathbf{A})]^2}\right]} \\
&= \sqrt{\frac{1}{E[\bar{h}_n(\mathbf{A})]^2} - \frac{2}{E[\bar{h}_n(\mathbf{A})]}E\left[\frac{1}{E_{\mathbf{P}(\mathbf{A})}[\bar{h}_n(\mathbf{A})]}\right] + E\left[\frac{1}{E_{\mathbf{P}(\mathbf{A})}[\bar{h}_n(\mathbf{A})]^2}\right]} \\
&\simeq \sqrt{\frac{1}{E[\bar{h}_n(\mathbf{A})]^2} - \frac{2}{E[\bar{h}_n(\mathbf{A})]}\left(\frac{1}{E[\bar{h}_n(\mathbf{A})]} + \frac{1}{|\mathbf{P}(\mathbf{A})|}\frac{Var[\bar{h}_n(\mathbf{A})]}{E[\bar{h}_n(\mathbf{A})]^3}\right) + E\left[\frac{1}{E_{\mathbf{P}(\mathbf{A})}[\bar{h}_n(\mathbf{A})]^2}\right]} \\
&= \sqrt{E\left[\frac{1}{E_{\mathbf{P}(\mathbf{A})}[\bar{h}_n(\mathbf{A})]^2}\right] - \frac{1}{E[\bar{h}_n(\mathbf{A})]^2} - \frac{2}{|\mathbf{P}(\mathbf{A})|}\frac{Var[\bar{h}_n(\mathbf{A})]}{E[\bar{h}_n(\mathbf{A})]^4}}.
\end{aligned} \tag{B.1}$$

The third-order Taylor expansion of $f(X) = 1/X^2$ around $E[X]$ is derived as

$$\frac{1}{X^2} \simeq \frac{1}{E[X]^2} - \frac{2}{E[X]^3}(X - E[X]) + \frac{3}{E[X]^4}(X - E[X])^2 - \frac{4}{E[X]^5}(X - E[X])^3. \tag{B.2}$$

We can then obtain

$$E\left[\frac{1}{E_{\mathbf{P}(\mathbf{A})}[\bar{h}_n(\mathbf{A})]^2}\right] \simeq \frac{1}{E[E_{\mathbf{P}(\mathbf{A})}[\bar{h}_n(\mathbf{A})]]^2} + \frac{3Var[E_{\mathbf{P}(\mathbf{A})}[\bar{h}_n(\mathbf{A})]]}{E[E_{\mathbf{P}(\mathbf{A})}[\bar{h}_n(\mathbf{A})]]^4}, \tag{B.3}$$

by taking the expectations and substituting $E_{\mathbf{P}(\mathbf{A})}[\bar{h}_n(\mathbf{A})]$ for X. If the probe vehicles are randomly sampled from all of the vehicles, this can be transformed to

$$E\left[\frac{1}{E_{\mathbf{P}(\mathbf{A})}[\bar{h}_n(\mathbf{A})]^2}\right] \simeq \frac{1}{E[\bar{h}_n(\mathbf{A})]^2} + \frac{3}{|\mathbf{P}(\mathbf{A})|}\frac{Var[\bar{h}_n(\mathbf{A})]}{E[\bar{h}_n(\mathbf{A})]^4}. \tag{B.4}$$

From (B.1) and (B.4), the precision can be approximated as

$$\mathrm{RMSE}(\hat{q}(\mathbf{A})) \simeq \frac{1}{E[\bar{h}_n(\mathbf{A})]^2}\sqrt{\frac{Var[\bar{h}_n(\mathbf{A})]}{|\mathbf{P}(\mathbf{A})|}}. \tag{B.5}$$

Appendix C: Spacing measurement method emploied in the experiment

This appendix describes details of the spacing measurement method employed for the experiment (c.f., Section 3.2).

The spacing s was estimated from images taken by the probe vehicles based on the following equation assuming that the road is not curved.

$$s = \frac{2wp_0}{p\tan(\theta_0/2)} + l, \tag{C.1}$$

where w is the actual body width of the leading vehicle, p_0 is the width of the image, p is the apparent size of the body width of the leading vehicle in the image, θ_0 is the horizontal angle of view of the camera, and l is the actual body length of the leading vehicle. Here, the variables p_0 and θ_0 were known. The actual body width w was assumed to be 1.92 m. This assumption comes from prior knowledge on the average width of a standard vehicle (1.8 m), large vehicle (2.4 m), and the average ratio of large vehicles on the route (20%). The actual body length l was assumed to be the same as that of the probe vehicles (5 m). Variable p was manually measured from the images. If these variables have errors (i.e., wrong assumptions on w and l, measurement error in p), the estimated spacing may be biased. The biases can be explained as follows. Let r_3 and r_4 be positive coefficients describing biases of body width and length respectively. In general, if an assumed body width is r_3 times the actual one, the spacing will be measured about r_3 times the actual spacing. If an assumed body length is r_4 times the actual one, the spacing will be measured $(a + r_4 l)/(a + l)$ times the actual spacing; where a is actual rear to front headway and l is actual body length. If the spacing was not measurable (i.e., the leading vehicle was not visible), a value of 100 m was assumed for the value. The most frequently appeared reason of the failure in spacing measurement was too large distance to leading vehicles. Therefore, the large value that is close to the maximum detectable range was substituted for the missing spacing data. Such cases occurred for 1.86% of all the data.

Appendix D: Estimation results of various scenarios

Table D.1 shows estimation bias and precision of the proposed method in the experiment for various scenarios, including resolution of 1 min which is often utilized for traffic management and control. The tendencies described in the Section 4.2 can be found in these scenarios.

Table D.1: Precision and bias indices over scenarios.

Senario Parameters			Flow [veh/h]		Density [veh/km]		Speed [km/h]	
P	Δt [min]	Δx [km]	RMSPE($\hat{q}$)	Bias($\hat{q}$)	RMSPE($\hat{k}$)	Bias($\hat{k}$)	RMSPE($\hat{v}$)	Bias($\hat{v}$)
0.2%	1	0.5	61%	84.6	64%	−1.1	68%	1.8
0.2%	1	4.0	50%	−0.9	63%	−1.0	55%	4.0
0.2%	1	11.0	36%	40.3	54%	4.9	60%	4.0
0.2%	5	0.5	43%	44.3	49%	−0.1	43%	0.4
0.2%	5	4.0	32%	−120.6	47%	−0.1	42%	0.3
0.2%	5	11.0	33%	−48.7	45%	2.1	31%	−0.3
0.2%	60	0.5	25%	−59.9	28%	−2.9	23%	0.7
0.2%	60	4.0	27%	−10.4	28%	1.7	13%	−1.8
0.2%	60	11.0	16%	−159.0	13%	−1.1	11%	−3.1
1.0%	1	0.5	54%	82.0	57%	0.4	45%	0.6
1.0%	1	4.0	36%	−75.9	49%	3.8	44%	−1.2
1.0%	1	11.0	22%	−94.8	32%	2.2	25%	−2.1
1.0%	5	0.5	43%	21.1	47%	0.2	25%	−0.4
1.0%	5	4.0	25%	−111.2	34%	1.2	24%	−2.4
1.0%	5	11.0	18%	−155.8	22%	0.2	18%	−3.1
1.0%	60	0.5	15%	−121.4	17%	−3.5	13%	−0.5
1.0%	60	4.0	13%	−147.9	8%	−2.2	8%	−2.3
1.0%	60	11.0	12%	−134.5	5%	−0.7	9%	−2.8
3.5%	1	0.5	40%	−26.5	43%	−1.8	34%	−0.1
3.5%	1	4.0	20%	−116.8	28%	0.2	25%	−1.8
3.5%	1	11.0	15%	−125.3	19%	−0.4	17%	−2.1
3.5%	5	0.5	26%	−82.4	28%	−2.6	18%	−0.7
3.5%	5	4.0	16%	−154.8	17%	−1.5	15%	−2.5
3.5%	5	11.0	14%	−151.9	13%	−0.6	13%	−3.0
3.5%	60	0.5	14%	−147.1	15%	−4.2	12%	−0.6
3.5%	60	4.0	13%	−158.6	6%	−2.6	8%	−2.3
3.5%	60	11.0	13%	−161.4	3%	−1.4	10%	−3.0

Appendix E: Precision comparison with penetration rate-based estimation method

As a benchmark of the proposed method's estimation precision, comparison with other estimation method, namely penetration rate-based estimation method, is described in this appendix.

The penetration rate-based method estimates flow $\hat{q}_{\mathrm{pr}}$ and density $\hat{k}_{\mathrm{pr}}$ from the probe vehicle data and an average probe vehicle penetration rate during the experiment. The probe vehicle data was the same as the data collected in the experiment. The penetration rate was exogenously given based on the probe vehicle data and the detector data. The penetration rate-based estimators were defined as follows:

$$\hat{q}_{\mathrm{pr}} = \frac{\sum_{n\in\mathbf{P}(\mathbf{A})} d_n(\mathbf{A})}{P|\mathbf{A}|}, \tag{E.1}$$

$$\hat{k}_{\mathrm{pr}} = \frac{\sum_{n\in\mathbf{P}(\mathbf{A})} t_n(\mathbf{A})}{P|\mathbf{A}|}, \tag{E.2}$$

where P is the average probe vehicle penetration rate.

Table E.1 summarizes the estimation and comparison results. PoI($\hat{\theta}$), which was calculated as PoI($\hat{\theta}$) = (RMSPE($\hat{\theta}$) − RMSPE($\hat{\theta}_{\mathrm{pr}}$))/RMSPE($\hat{\theta}_{\mathrm{pr}}$), represents the percentage of improvement of the spacing-based estimator $\hat{\theta}$ compared with the penetration rate-based estimator $\hat{\theta}_{\mathrm{pr}}$—positive value of PoI($\hat{\theta}$) means that the spacing-based estimator is better precision. According to Table E.1, the spacing-based estimators

always had better precision than the penetration rate-based ones, especially at higher resolution scenarios. It implied that the proposed method has better performance compared to other GPS-equipped probe vehicle-based traffic state estimation methods where reliable and detailed external knowledge (e.g., detector data, an FD) is not available.

Table E.1: Precision comparison with penetration rate-based estimation method.

Scenario parameters			Flow			Density		
P	Δt [min]	Δx [km]	RMSPE($\hat{q}$)	RMSPE($\hat{q}_{\text{pr}}$)	PoI($\hat{q}$)	RMSPE($\hat{k}$)	RMSPE($\hat{k}_{\text{pr}}$)	PoI($\hat{k}$)
0.2%	5	0.5	43%	178%	76%	49%	188%	74%
0.2%	60	4.0	27%	53%	50%	28%	55%	49%
3.5%	5	0.5	26%	47%	43%	28%	51%	45%
3.5%	60	4.0	13%	16%	22%	6%	14%	56%

References

Asakura, Y., Hato, E., 2004. Tracking survey for individual travel behaviour using mobile communication instruments. Transportation Research Part C: Emerging Technologies 12, 273–291. doi:http://dx.doi.org/10.1016/j.trc.2004.07.010.

Coifman, B., Beymer, D., McLauchlan, P., Malik, J., 1998. A real-time computer vision system for vehicle tracking and traffic surveillance. Transportation Research Part C: Emerging Technologies 6, 271–288. doi:http://dx.doi.org/10.1016/S0968-090X(98)00019-9.

Daganzo, C.F., 1997. Fundamentals of transportation and traffic operations. Pergamon Oxford.

Edie, L., 1963. Discussion of traffic stream measurements and definitions, in: Almond, J. (Ed.), Proceedings of the 2nd International Symposium on the Theory of Traffic Flow, pp. 139–154.

Geroliminis, N., Daganzo, C.F., 2008. Existence of urban-scale macroscopic fundamental diagrams: Some experimental findings. Transportation Research Part B: Methodological 42, 759–770. doi:10.1016/j.trb.2008.02.002.

Herrera, J.C., Work, D.B., Herring, R., Ban, X.J., Jacobson, Q., Bayen, A.M., 2010. Evaluation of traffic data obtained via GPS-enabled mobile phones: The Mobile Century field experiment. Transportation Research Part C: Emerging Technologies 18, 568–583. doi:http://dx.doi.org/10.1016/j.trc.2009.10.006.

Hilbert, E.E., Rennie, P., Kneidl, W., 1980. A sensor for control of arterials and networks. Vehicular Technology, IEEE Transactions on 29, 208–215. doi:10.1109/T-VT.1980.23842.

Mehran, B., Kuwahara, M., Naznin, F., 2012. Implementing kinematic wave theory to reconstruct vehicle trajectories from fixed and probe sensor data. Transportation Research Part C: Emerging Technologies 20, 144–163. doi:10.1016/j.trc.2011.05.006.

Murakami, E., Wagner, D., 1999. Can using global positioning system (GPS) improve trip reporting? Transportation Research Part C: Emerging Technologies 7, 149–165. doi:http://dx.doi.org/10.1016/S0968-090X(99)00017-0.

Nanthawichit, C., Nakatsuji, T., Suzuki, H., 2003. Application of probe-vehicle data for real-time traffic-state estimation and short-term travel-time prediction on a freeway. Transportation Research Record: Journal of the Transportation Research Board 1855, 49–59.

National Highway Traffic Safety Administration, 2013. Preliminary statement of policy concerning automated vehicles. Press release.

Papageorgiou, M., Diakaki, C., Dinopoulou, V., Kotsialos, A., Wang, Y., 2003. Review of road traffic control strategies. Proceedings of the IEEE 91, 2043–2067. doi:10.1109/JPROC.2003.819610.

Quddus, M.A., Ochieng, W.Y., Noland, R.B., 2007. Current map-matching algorithms for transport applications: State-of-the art and future research directions. Transportation Research Part C: Emerging Technologies 15, 312–328. doi:http://dx.doi.org/10.1016/j.trc.2007.05.002.

Reddy, S., Mun, M., Burke, J., Estrin, D., Hansen, M., Srivastava, M., 2010. Using mobile phones to determine transportation modes. ACM Transactions on Sensor Networks (TOSN) 6, 13.

Redmill, K., Coifman, B., McCord, M., Mishalani, R., 2011. Using transit or municipal vehicles as moving observer platforms for large scale collection of traffic and transportation system information, in: Intelligent Transportation Systems (ITSC), 2011 14th International IEEE Conference on, pp. 1089–1095. doi:10.1109/ITSC.2011.6083132.

Saneyoshi, K., 1996. Drive assist system using stereo image recognition, in: Proceedings of the IEEE Intelligent Vehicles Symposium, IEEE. pp. 230–235.

Seo, T., Kusakabe, T., Asakura, Y., 2012. Traffic state estimation with observed spacing data by probe vehicles, in: Proceedings of Infrastructure Planning 46. (in Japanese).

Seo, T., Kusakabe, T., Asakura, Y., 2013. Traffic flow monitoring utilizing on-vehicle devices of spacing measurement, in: 2nd Symposium of the European Association for Research in Transportation.

Shiraishi, T., Akahane, H., Morita, H., Horiguchi, R., 2012. Development of a method for correcting bias in urban expressway traffic detectors, in: Proceedings of the 32nd Conference of Japan Society of Traffic Engineers. (in Japanese).

Wardrop, J.G., Charlesworth, G., 1954. A method of estimating speed and flow of traffic from a moving vehicle, in: ICE Proceedings: Engineering Divisions, Thomas Telford. pp. 158–171.

Yokoi, K., Suzuki, Y., Sato, T., Abe, T., Toda, H., Ozaki, N., 2013. A camera-based probe car system for traffic condition estimation, in: Proceedings of 20th ITS World Congress.

Yuan, Y., van Lint, J.W.C., Wilson, R.E., van Wageningen-Kessels, F., Hoogendoorn, S.P., 2012. Real-time Lagrangian traffic state estimator for freeways. IEEE Transactions on Intelligent Transportation Systems 13, 59–70.

Zito, R., D'Este, G., Taylor, M., 1995. Global positioning systems in the time domain: How useful a tool for intelligent vehicle-highway systems? Transportation Research Part C: Emerging Technologies 3, 193–209. doi:10.1016/0968-090X(95)00006-5.